Nonlinear interaction between bulk vortices and the interface in the incompressible Richtmyer-Meshkov instability

Chihiro Matsuoka

MATSUOKA C. (2020). Nonlinear interaction between bulk vortices and the interface in the incompressible Richtmyer-Meshkov instability. *High Energy Density Physics*. 36, 100834. Doi:1016/j.hedp.2020.100834

Nonlinear interaction between bulk vortices and the interface in the incompressible Richtmyer-Meshkov instability

Chihiro Matsuoka[a,b,c]

[a] *Laboratory of Applied Mathemetics, Graduate School of Engineering, Osaka City University, 3-3-138, Sugimoto, Sumiyoshi, Osaka 558-8585, Japan*

[b] *Nambu Yoichiro Institute of Theoretical and Experimental Physics (NITEP), Osaka City University*

[c] *Osaka City University Advanced Mathematical Institute (OCAMI), Osaka City University*

Abstract

Nonlinear interaction between bulk point vortices and the interface in the incompressible Richtmyer-Meshkov instability (RMI) is investigated theoretically and numerically. When the strength of point vortices are large enough, they interact with the original vorticity existing on the vortex sheet and create new vortex cores. These vortex cores roll up like mushrooms, and a very complicated interfacial structure is formed at the final stage. It is shown that satellite bubbles and spikes are created in the neighborhood of original bubbles and spikes when bulk point vortices approach the interface. The shape of an interface is largely deformed by the existence of bulk point vortices; however, the asymptotic growth rate of the bubble and spike is almost the same as the one for pure RMI without point vortices.

Keywords: Richtmyer-Meshkov instability, bulk point vortices, vortex sheet

Email address: cmatsuoka@osaka-cu.ac.jp (Chihiro Matsuoka[a,b,c])

1. Introduction

The study of vortex sheets is important in various areas in fluid dynamics and plasma physics. The numerical method, such as the vortex method [1] that is one of the boundary integral method has developed as a high-precision computational method to investigate the Kelvin-Helmholtz instability (KHI) [2, 3]. Extending this vortex method to the fluid systems with density stratification, Matsuoka et al. [4, 5, 6] and Sohn et al. [7] succeeded to capture the long-time behavior of the vortex sheet motion with density stratification such as the Rayleigh-Taylor instability (RTI) or the Ricytmyer-Meshukov instability (RMI) [8, 9]. These works assume that there are no vortices in bulk. However, in problems of practical importance, there exist bulk vortices, and they strongly interact with an interface or a vortex sheet.

When a shock wave crosses interfaces in RMI, the reflected shocks or rarefaction waves occur at the interfaces. Defects in a target [10] also cause the generation of point-like vortices in bulk when shocks pass through. The vorticity or strength of these defect-induced bulk vortices is not necessarily weak, and they can lead the system to a turbulent state by interacting with the non-uniform vortex sheet in RMI. Therefore, it is important for controlling RMI to know the behavior of the interface or the vortex sheet coexisting with bulk vortices.

The velocity perturbations associated with RMI that create non-uniform vorticity on the interface depend on various parameters before a shock hits a corrugated interface, such as incident shock strength, initial corrugation amplitude, initial density jump at the interface, and thermodynamic properties of the fluids. The bulk vorticity also depends on those parameters. Moreover, their dependence is nonlinear. Therefore, it is difficult to present the concrete dependence on the parameters in simple expressions, even if that is a qualitative one. However, the following facts are known: the velocity shear at the interface and bulk vortices are in general stronger for larger corrugation amplitude, and stronger shocks, and/or compressible fluids [11, 12, 13, 14, 15, 16, 17]. In the current study, approximating the bulk vortices and the interface in RMI as point vortices [18, 19] and a vortex sheet [4, 20, 21], respectively, we theoretically investigate the nonlinear interaction between bulk vortices and an interface with strong non-uniform vorticity in RMI.

When the point vortices approach the density interface, they create a new velocity shear, and the velocity shear produces non-uniform vorticity on the

interface. The non-uniform vorticity created by point vortices interacts with the original vorticity on the interface, and finally, a very complicated vortex sheet structure appears in the system. In numerical results, we show that the bulk point vortices create satellite bubbles and spikes in the neighborhood of original bubbles and spikes. We also present the growth rates of bubbles and spikes when the bulk point vortices exist and compare those with the one without point vortices.

This paper is organized as follows. We provide the mathematical model when an interface with non-uniform velocity shear and bulk point vortices coexist in the system and derive the governing equations for describing the motion of them in Section 2. In Section 3, we present some numerical results for the motion of the vortex sheet and point vortices in RMI. Section 4 is devoted to to conclusion.

2. Governing equations

For ideal plasmas, the shock ripples will decrease to zero when the shocks separate from the contact surface of which distance greater than perturbation wavelength [27]. We assume that enough time has passed after the passage of the shock, and the system becomes incompressible. In this incompressible stage, we consider a fluid interface with density and tangential velocity jumps in two-dimensional inviscid flows. We also assume that the fluid is irrotational except the interface and point vortices.

Now we parameterize points on the interface $\boldsymbol{x} = \boldsymbol{X}$ as

$$\boldsymbol{X}(e,t) = [X(e,t), Y(e,t)]$$

using a Lagrangian parameter e ($-\pi \le e \le \pi$). Now we assume the periodicity in the x direction. When bulk vortices exist in the system, the vortex induced fluid velocity $\boldsymbol{W}$ at an arbitrary point $\boldsymbol{x} = (x, y)$ is given as the sum of the two velocities

$$\boldsymbol{W} = \boldsymbol{W}_s + \boldsymbol{W}_p, \tag{1}$$

in which $\boldsymbol{W}_s = (W_{s,x}, W_{s,y})$ is the velocity by the contribution from the interface

$$\begin{aligned} W_{s,x}(x,y) = & -\frac{1}{4\pi}\int_{-\pi}^{\pi} \frac{\gamma(e',t)s_e(e',t)\sinh(y-Y(e',t))}{\cosh(y-Y(e',t))-\cos(x-X(e',t))}de', \\ W_{s,y}(x,y) = & \frac{1}{4\pi}\int_{-\pi}^{\pi} \frac{\gamma(e',t)s_e(e',t)\sin(x-X(e',t))}{\cosh(y-Y(e',t))-\cos(x-X(e',t))}de', \end{aligned} \tag{2}$$

and $\boldsymbol{W}_p = (W_{p,x}, W_{p,y})$ is the velocity by the contribution from bulk vorticies

$$\begin{aligned} W_{p,x}(x,y) = & -\frac{1}{4\pi}\sum_{j=1}^{N}\frac{\gamma_{p,j}\sinh(y-y_{p,j}(t))}{\cosh(y-y_{p,j}(t))-\cos(x-x_{p,j}(t))}, \\ W_{p,y}(x,y) = & \frac{1}{4\pi}\sum_{j=1}^{N}\frac{\gamma_{p,j}\sin(x-x_{p,j}(k))}{\cosh(y-y_{p,j}(t))-\cos(x-x_{p,j}(t))}, \end{aligned} \tag{3}$$

where $\boldsymbol{\gamma} = \boldsymbol{u}_1 - \boldsymbol{u}_2$, and $\gamma = \boldsymbol{\gamma}\cdot\boldsymbol{t} = \partial\Gamma/\partial s$ denotes the (true) vortex sheet strength derived from the circulation $\Gamma \equiv \phi_1 - \phi_2$, in which ϕ_i $(i = 1, 2)$ is the velocity potential related to the fluid velocity $\boldsymbol{u}_i$ as $\boldsymbol{u}_i = \nabla\phi_i$, and s is the arclength and $\boldsymbol{t}$ is the unit tangential vector of the interface, respectively. Here, the subscript e denotes the differentiation with respect to e and $s_e = \sqrt{X_e^2 + Y_e^2}$. We take the principal value of the integral (2) when the point (x, y) is on the interface: $(x, y) = (X, Y)$. Equation (2) corresponds to the Birkhoff-Rott equation [22, 23, 24] if (x, y) is on the interface. Here, $\gamma_{p,j}$ and N denote the strength of point vortex j and the number of point vortices, respectively. The strength of point vortex j is defined as $\gamma_{p,j} = \Gamma_{p,j}/\lambda$, where $\Gamma_{p,j}$ is the circulation of point vortex j and λ $(= 2\pi)$ is the normalized wavelength of the initial perturbation of the vortex sheet. Traditionally, the circulation $\Gamma_{p,j}$ is called the strength of point vortex j [18].

We define the interfacial velocity $\boldsymbol{u}^+$ of a Lagrangian point labelled by e as

$$\boldsymbol{u}^+(e,t) = \boldsymbol{W}|_{\boldsymbol{x}=\boldsymbol{X}} + \frac{\tilde{\alpha}\gamma}{2}\boldsymbol{t},$$

where $\boldsymbol{W}|_{\boldsymbol{x}=\boldsymbol{X}} \equiv (U, V)$ corresponds to the average velocity $(\boldsymbol{u}_1 + \boldsymbol{u}_2)/2$ at the interface and $\tilde{\alpha}$ is an artificial parameter [4] depending on the Atwood number A defined by $A = (\rho_2 - \rho_1)/(\rho_1 + \rho_2)$. Here, ρ_i $(i = 1, 2)$ is the fluid densitiy and we denote $i = 1$ $(i = 2)$ as the lower (upper) fluid, in which we assume that $i = 1$ $(i = 2)$ is the heavier (lighter) fluid. Equating $\boldsymbol{u}^+$ with the evolution of the interface, we have the interfacial velocity for the Lagrangian motion as

$$\frac{\mathrm{d}\boldsymbol{X}}{\mathrm{d}t} = \boldsymbol{W}|_{\boldsymbol{x}=\boldsymbol{X}} + \frac{\tilde{\alpha}\gamma}{2}\boldsymbol{t}, \tag{4}$$

where

$$\frac{\mathrm{d}}{\mathrm{d}t} = \frac{\partial}{\partial t} + \boldsymbol{u}^+\cdot\nabla$$

is the Lagrangian derivative in the frame moving with the interface.

A point vortex velocity is given by substituting its location $\boldsymbol{x} = \boldsymbol{x}_{p,i}$ into (1):

$$\frac{\mathrm{d}\boldsymbol{x}_{p,i}}{\mathrm{d}t} = \boldsymbol{W}_s|_{\boldsymbol{x}=\boldsymbol{x}_{p,i}} + \boldsymbol{W}_p|_{\boldsymbol{x}=\boldsymbol{x}_{p,i}} \ (i = 1, 2, \cdots N), \tag{5}$$

where the term of $j = i$ (own contribution) in the integral (3) is excluded from the summation.

Differentiating the Bernoulli equation obtained from the Euler equation with respect to e [4], we obtain the evolution equation for the sheet strength γ as follows:

$$\begin{aligned} \frac{\mathrm{d}\gamma}{\mathrm{d}t} &= \frac{2A}{s_e}\left(X_e\frac{\mathrm{d}U}{\mathrm{d}t} + Y_e\frac{\mathrm{d}V}{\mathrm{d}t}\right) \\ &- \frac{(1+\tilde{\alpha}A)\gamma}{s_e^2}(X_eU_e + Y_eV_e) + \frac{A+\tilde{\alpha}}{4s_e}(\gamma^2)_e. \end{aligned} \tag{6}$$

Since we assume the potential flow, the Laplace equation $\triangle\phi_i = 0$ $(i = 1, 2)$ holds for the velocity potential ϕ_i in each fluid region i. Solving equations (4), (5), and (6) simultaneously by taking the integrals (2) and (3) into account, we can determine the motion of the interface and bulk point vortices.

3. Numerical results

In numerical calculations, all physical quantities are normalized by the wavenumber k and the initial velocity shear of the vortex sheet v_{lin}, the linear growth rate of RMI [12, 11]

$$v_{lin} = \frac{\rho_1\delta v_1^* - \rho_2\delta v_2^*}{\rho_1 + \rho_2}, \tag{7}$$

so that they are dimensionless, where $\delta v_{1,2}^*$ represents the transverse velocities immediately after the shock-interface interaction in RMI [11, 12, 25]. From now on, the dimensionless variables space $k\boldsymbol{x}$, time $kv_{lin}t$, circulation of vortex sheet $k\Gamma/v_{lin}$, vortex sheet strength γ/v_{lin}, circulation of point vortex j $k\Gamma_{p,j}/v_{lin}$, and strength of point vortex $\gamma_{p,j}/v_{lin}$ $(j = 1, 2\cdots N)$ are used as $\boldsymbol{x}$, t, Γ, γ, $\Gamma_{p,j}$, and $\gamma_{p,j}$ $(j = 1, 2\cdots N)$.

In order to avoid the singularity formation of the vortex sheet [4, 26], we use a regularized parameter δ introduced by Krasny [3] for the numerical

integration of (2) on the sheet. Here, we select $\delta = 0.15$ [4, 20, 21]. We fix the Atwood number A and the artificial parameter $\tilde{\alpha}$ in (4) and (6) as $A = -0.2$ ($\rho_2 < \rho_1$) and $\tilde{\alpha} = A^2$, respectively throughout the paper.

In order to calculate the evolution of the interface, we adopt a point insertion scheme [3, 7]. Since the grid number M increases as the vortex sheet evolves, we need to vary the time step in accordance with that. In the calculation, we set the time step $\triangle t$ so that $\triangle t = \triangle t_0/2^{m-1}$ for $M \geq 2^{(m-1)}M_0$ ($m = 1, 2, 3\cdots$), where M_0 and $\triangle t_0$ are the grid number and time step at $t = 0$, respectively. We select $M_0 = 256$ and $\triangle t_0 = 0.001$ throughout the paper.

The initial condition of the interface is given as follows [4]:

$$\begin{aligned} x(e,0) &= e, \quad (-\pi \leq e \leq \pi) \\ y(e,0) &= 0, \\ \gamma(e,0) &= -2\sin e. \end{aligned} \tag{8}$$

It is reported by Cobos-Campos et al. that bulk vortices are generated behind the rippled oscillating shocks corresponding to the transmitted and reflected shocks in the linear theory [27, 28]. For our initial condition (8), those positions correspond to $x \sim \pm\pi/2$. Here, we set the initial distribution of four point vortices close to the vortex sheet so that two point vortices are placed over the vortex sheet and the other two vortices under the sheet.

The initial position of four vortices is given as

$$\begin{aligned} &x_{p,1}(0) = -\frac{\pi}{2},\ y_{p,1}(0) = \frac{\pi}{4},\ \gamma_{p,1}(0) = \gamma_1, \\ &x_{p,2}(0) = -\frac{\pi}{2},\ y_{p,2}(0) = -\frac{\pi}{4},\ \gamma_{p,2}(0) = \gamma_2, \\ &x_{p,3}(0) = \frac{\pi}{2},\ y_{p,3}(0) = \frac{\pi}{4},\ \gamma_{p,3}(0) = \gamma_3, \\ &x_{p,4}(0) = \frac{\pi}{2},\ y_{p,4}(0) = -\frac{\pi}{4},\ \gamma_{p,4}(0) = \gamma_4. \end{aligned} \tag{9}$$

For the initial distributions of the strength of point vortices, we consider the following two cases. The first one (Case 1) is given by

$$\gamma_1 = \gamma_2 = -\gamma_0, \quad \gamma_3 = \gamma_4 = \gamma_0, \tag{10}$$

and the second one (Case 2) is given as

$$\gamma_1 = \gamma_4 = \gamma_0, \quad \gamma_2 = \gamma_3 = -\gamma_0, \tag{11}$$

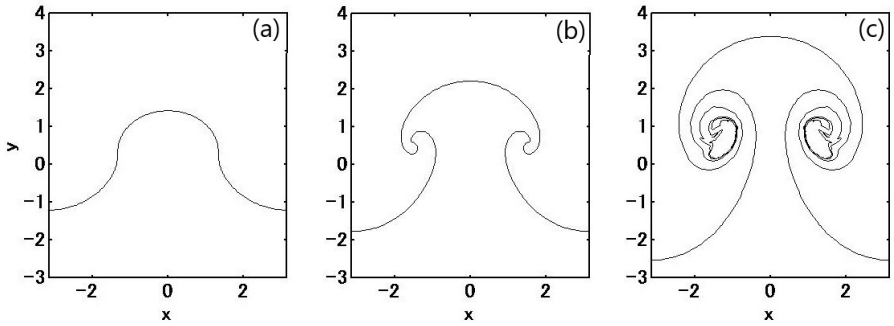

Figure 1: Interfacial structures of RMI without bulk point vortices at $t =$ (a) 2, (b) 4, and (c) 10.1885.

where we set $\gamma_0 = 1$ throughout the paper. As we see from the initial condition (8), two point vortices in Case 1 are set to the opposite sign of the sheet strength γ, where the maximum sheet strength in its absolute value appears in the neighbprhood of $x = \pi/2$ ($\gamma = -2$) and $x = -\pi/2$ ($\gamma = 2$) [refer to the initial condition (8) for γ and Fig. 2 (a)]. In Case 2, there are point vortices with different signs across the interface (refer to Fig. 3 (a)).

For comparison, we first provide the interfacial evolution of RMI without bulk point vortices in Fig. 1. The center of the roll-up is called the vortex core [29], where the vortex core in the region of $x < 0$ possesses strong positive sheet strength and the one in the region of $x > 0$ possesses strong negative sheet strength [4, 20].

Figure 2 shows the temporal evolution of the interface with bulk point vortices for Case 1 (10). In this case, the point vortex forms a new vortex core, and a new satellite mushroom is created. The blue (red) point vortices approach the vortex sheet with the strong positive (negative) sheet strength while rotating [(a) - (b)] and form new vortex cores with those sheet strengths, in which process, the vortex sheet with strong sheet strength splits into four cores (two in the neighborhood of spike and the other two in the neighborhood of bubble). These vortex cores make pseudo vortex pairs with those point vortices, and new mushrooms of which number coincides with that of point vortices appear on the sheet [(c) - (f)]. We see that the interfacial structure becomes extremely complicated due to the presence of point vortices compared to that without point vortices (Fig. 1).

Figure 3 shows the interfacial structures for Case 2 (11), in which the

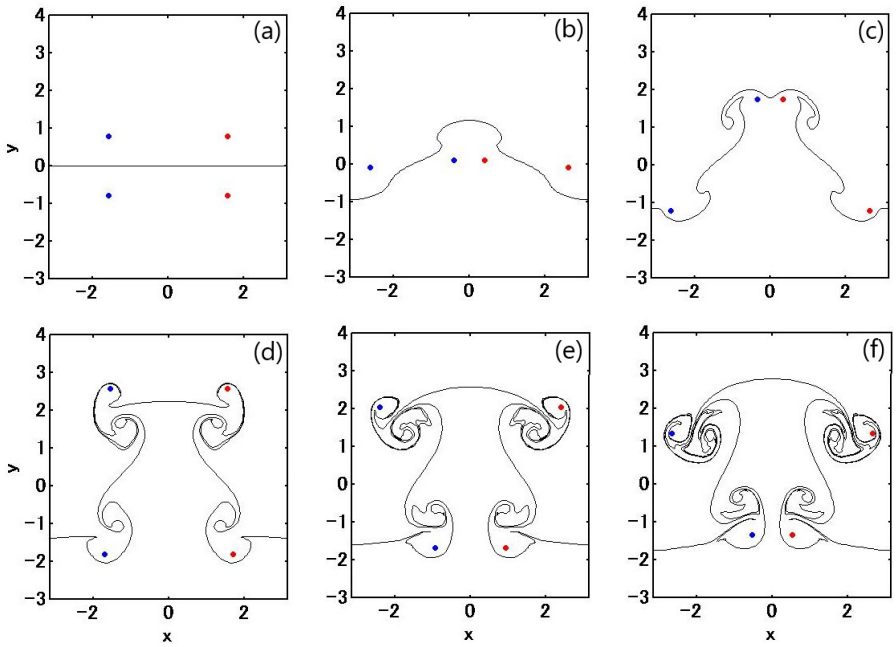

Figure 2: Interfacial structures with bulk point vortices given by Case 1 (10) at $t =$ (a) 0, (b) 2, (c) 4, (d) 6.9155, (e) 8.7765, and (f) 10.265, where the red and blue points denote the strength of point vortices having positive ($\gamma_0 = 1$, counter-clockwise rotation) and negative ($\gamma_0 = -1$, clockwise rotation) signs, respectively.

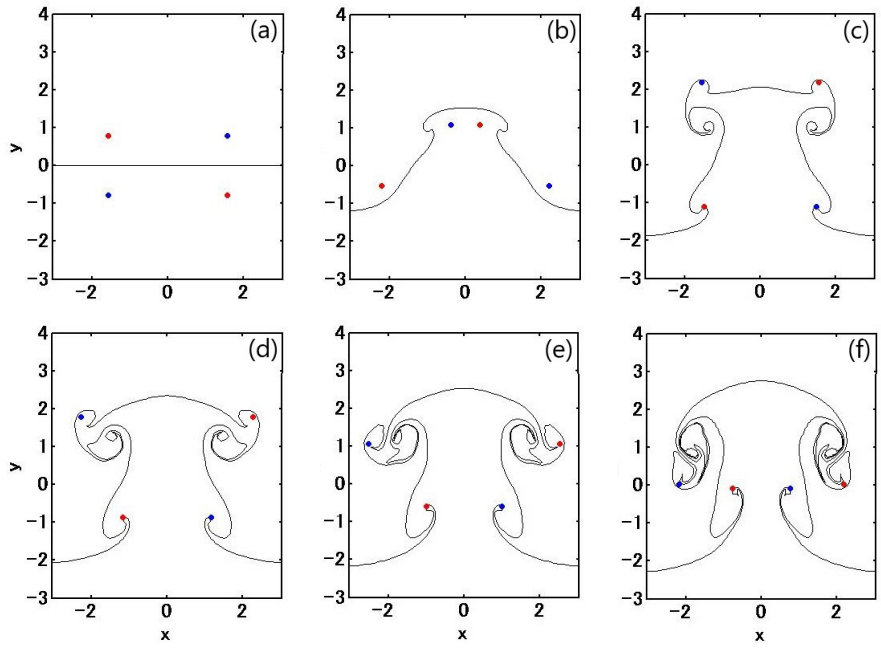

Figure 3: Interfacial structures with bulk point vortices given by Case 2 (11) at $t =$ (a) 0, (b) 2, (c) 4, (d) 5, (e) 5.75, and (f) 6.73, where the colors of point vortices are the same as those in Fig. 2.

signs of the point vortices over the sheet (the lighter fluid) are opposite to those in the initial condition (10). In this case, the motion of two point vortices $(p, 2)$ and $(p, 4)$ [refer to (9)] in the heavier fluid at the early stage is the same as its background fluid motion due to RMI. Therefore, their distance becomes closer, and they form a new pair and go upwards with the heavier fluid. Since the sign of these point vortices $(p, 2)$ and $(p, 4)$ (in the heavier fluid) is opposite to that of the velocity shear on the sheet, these vortices make the pseudo vortex pairs with the vortex cores on the sheet (b) approaching the sheet, and two local mushrooms are created on both sides of the spike of the original mushroom [(b) - (f)].

The other two point vortices $(p, 1)$ and $(p, 3)$ initially located over the sheet move downwards with the background lighter fluid separating each other. Even when the vortices get close to the sheet, they do not induce vortex cores because they have the same signs with the velocity shear on the sheet. In this case, the point vortices and the sheet begin to rotate. As a result, the lighter fluid with these vortices penetrates the heavier fluid, as seen in (d) - (f). Three mushrooms are finally formed (the original large mushroom and two satellite mushrooms created on both sides of the spike of the original mushroom) for the initial condition (11).

We show the temporal evolution of original bubbles ($x = \pm\pi$) and spikes ($x = 0$) in Fig. 4, in which (b) and (c) denote the growth rate of bubbles and spikes. The behavior of bubble amplitude and velocity (growth rate) of the interface without point vortices (black line) and those of Case 2 (red line) are almost the same. On the other hand, the growth rate of the bubble in Case 1 (blue line) is quite different from the other two lines. This is due to the creation of satellite bubbles [refer to Fig. 2 (c)], which causes the slow down of the original bubble growth rate. At the same time as the creation of satellite bubbles, satellite spikes also appear in the neighborhood of the original spike for Case 1 ($t \sim 4$), where the growth rate of spike slows down as depicted in Fig. 4 (c). This situation is also found in Case 2 (red line) when the satellite spikes are created [refer to Fig. 3 (b) - (c)]. It should be noted that the asymptotic velocities of bubbles and spikes are almost the same for these three cases. This fact suggests that the asymptotic growth rate of bubble and spike in RMI is not affected by the existence of bulk point vortices, at least for the initial conditions 9, 10, and 11.

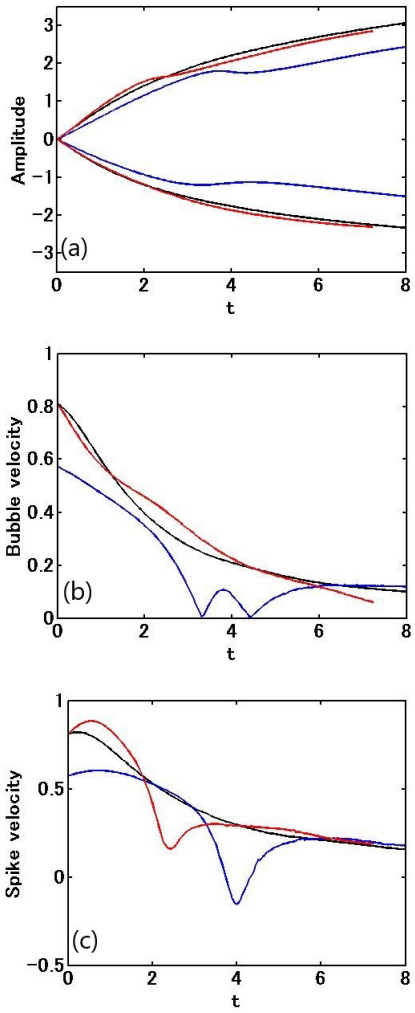

Figure 4: Temporal evolution of original bubbles and spikes: (a) amplitude of bubbles (vertical axis negative region) and spikes (vertical axis positive region), (b) absolute values of bubble velocities, (c) spike velocities, where the black, blue, and red lines denote the interface without bulk point vortices, Case 1 (10), and Case 2 (11), respectively.

4. Conclusion

We have investigated the interaction of the interface and bulk point vortices in RMI. We found that when the strength of the point vortex is the opposite sign to the local sheet strength (Case 1), new satellite bubbles and spikes are created in the neighborhood of the original bubble and spike as the point vortices approach the interface. When point vortices with different signs are initially located across the interface (Case 2), the point vortices with the same sign as the sheet strength rotate with the interface, while the other vortices with the different sign as the sheet strength create satellite spikes in the neighborhood of the original spike. The interfacial shape with bulk point vortices becomes complicated compared to the one without point vortices; however, the asymptotic growth rate of the original bubble and spike was unchanged within the initial conditions adopted in the present study. Although we selected the initial conditions of bulk point vortices following the result of the linear analysis [27, 28], other choices are possible for their locations. In that case, the asymptotic growth rate of bubbles and spikes may provide different result with the one presented here. We mention that the suppression of RMI by the existence of bulk vortices found in the linear analysis [27] was not found in the nonlinear stage, at least, in the initial conditions adopted in the present study.

Acknowledgements

The author would like to thank Professor K. Nishihara, J. G. Wouchuk, Dr. F. Cobos-Campos, and Dr. T. Sano for valuable discussions. This work was supported by Grant-in-Aid for Scientific Research (C) (Grant No. 17K05371 and Grant No. 18K03418) from the Japan Society for the Promotion of Science, the Osaka City University (OCU) Strategic Research Grant 2019 for top priority researches, and the joint research project of ILE, Osaka University.

References

[1] G-H. Cottet and P. D. Koumoutsakos, Vortex methods: theory and practice, Cambridge University Press, Cambridge, 2000.

[2] R. Krasny, A study of singularity formation in a vortex sheet by the point vortex approximation, J. Fluid Mech. 167 (1986) 65-93.

[3] R. Krasny, Computation of vortex sheet roll-up in the Trefftz plane, J. Fluid Mech. 184 (1987) 123-155.

[4] C. Matsuoka, K. Nishihara, Vortex core dynamics and singularity formations in incompressible Richtmyer-Meshkov instability, Phys. Rev. E 73 (2006) 026304, 74 049902(E).

[5] C. Matsuoka, K. Nishihara, Fully nonlinear evolution of a cylindrical vortex sheet in incompressible Richtmyer-Meshkov instability, Phys. Rev. E 73 (2006) 055304(R).

[6] C. Matsuoka, K. Nishihara, Analytical and numerical study on a vortex sheet in incompressible Richtmyer-Meshkov instability in cylindrical geometry, Phys. Rev. E 74 (2006) 066303.

[7] S. I. Sohn, D. Yoon, W. Hwang, Long-time simulations of the Kelvin-Helmholtz instability using an adaptive vortex method, Phys. Rev. E 82 (2010) 046711.

[8] R. D. Richtmyer, Taylor instability in shock acceleration of compressible fluids, Commun. Pure Appl. Math. 13 (1960) 297-319.

[9] E. E. Meshkov, Instability of the interface of two gases accelerated by a shock wave, Sov. Fluid Dynamics 4 (1969) 101-108.

[10] A. Nikroo, D. Woodhouse, Bounce coating induced domes on glow discharge polymer coated shells, Fusion Technology 35 (1999) 202-205.

[11] J. G. Wouchuk, K. Nishihara, Linear perturbation growth at a shocked interface, Phys. Plasmas 3 (1996) 3761-3776.

[12] J. G. Wouchuk, K. Nishihara, Asymptotic growth in the linear Richtmyer-Meshkov instability, Phys. Plasmas 4 (1997) 1028-1038.

[13] J. G. Wouchuk, Growth rate of the linear Richtmyer-Meshkov instability when a shock is reflected, Phys. Rev. E 63 (2001) 056303.

[14] M. Vandenboomgaerde, D. Souffland, C. Mariani, L. Biamino, G. Jourdan, L. Houas, An experimental and numerical investigation of the dependency on the initial conditions of the Richtmyer-Meshkov instability, Phys. Fluids 26 (2014) 024109.

[15] M. Stanic, R. F. Stellingwerf, J. T. Cassibry, S. I. Abarzhi, Scale coupling in Richtmyer-Meshkov flows induced by strong shocks, Phys. Plasmas 19 (2012) 082706.

[16] M. Stanic, R. F. Stellingwerf, J. T. Cassibry, S. I. Abarzhi, Non-uniform volumetric structures in Richtmyer-Meshkov flows, Phys. Fluids 25 (2013) 106107.

[17] Z. Dell, R. F. Stellingwerf, S. I. Abarzhi, Effect of initial perturbation amplitude on Richtmyer-Meshkov flows induced by strong shocks, Phys. Plasmas 22 (2015) 092711.

[18] H. Lamb, Hydrodynamics, Dover, New York, 1932.

[19] P. K. Newton, The N-vortex problem, Springer, New York, 2000.

[20] C. Matsuoka, K. Nishihara, T. Sano, Nonlinear dynamics of non-uniform current-vortex sheets in magnetohydrodynamic flows, J. Nonlinear Sci. 27 (2017) 531-572.

[21] C. Matsuoka, K. Nishihara, T. Sano, Nonlinear interfacial motion in magnetohydrodynamic flows, High Energy Density Phys. 31 (2019) 19-23.

[22] G. Birkhoff, Helmholtz and Taylor instability, Proc. Symp. Appl. Maths. Soc. 13 (1962) 55-76.

[23] N. Rott, Diffraction of a weak shock with vortex generation, J. Fluid Mech. 1 (1956) 111-128.

[24] P. G. Saffman, Vortex dynamics, Cambridge University Press, Cambridge, 1992.
.

[25] K. Nishihara, J. G. Wouchuk, C. Matsuoka, R. Ishizaki, V. V. Zhakhovskii, Richtmyer-Meshkov instability: theory of linear and nonlinear evolution, Phil.Trans. Roy. Soc. A 368 (2010) 1769-1807 (references therein).

[26] D. W. Moore, The spontaneous appearance of a singularity in the shape of an evolving vortex sheet, Proc. R. Soc. Lond. 365 (1979) 105-119.

[27] F. Cobos-Campos and J. G. Wouchuk, Analytical scalings of the linear Richtmyer-Meshkov instability when a shock is reflected, Phys. Rev. E 93 (2016) 053111.

[28] F. Cobos-Campos and J. G. Wouchuk, Analytical scalings of the linear Richtmyer-Meshkov instability when a rarefaction is reflected, Phys. Rev. E 96 (2017) 013102.

[29] N. Zabusky, Vortex paradigm for accelerated inhomogeneous flows: visiometrics for the Rayleigh-Taylor and Richtmyer-Meshkov environments, Ann. Rev. Fluid Mech. 31 (1999) 495-536.